Initiating and Monitoring the Evolution of Single Electrons Within Atom-Defined Structures

Mohammad Rashidi,[1,2,3,*] Wyatt Vine,[1,†] Thomas Dienel,[1,2,‡] Lucian Livadaru,[3] Jacob Retallick,[4] Taleana Huff,[1,3] Konrad Walus,[4] and Robert A. Wolkow[1,2,3]

[1]*Department of Physics, University of Alberta, Edmonton, Alberta, T6G 2J1, Canada*
[2]*Nanotechnology Initiative, Edmonton, AB, Canada, T6G 2M9*
[3]*Quantum Silicon, Edmonton, AB, Canada, T6G 2M9*
[4]*Department of Electrical and Computer Engineering, University of British Columbia, Vancouver, BC, V6T 1Z4, Canada*

(Received 21 November 2017; revised manuscript received 24 July 2018; published 15 October 2018)

Using a noncontact atomic force microscope, we track and manipulate the position of single electrons confined to atomic structures engineered from silicon dangling bonds on the hydrogen terminated silicon surface. An attractive tip surface interaction mechanically manipulates the equilibrium position of a surface silicon atom, causing rehybridization that stabilizes a negative charge at the dangling bond. This is applied to controllably switch the charge state of individual dangling bonds. Because this mechanism is based on short range interactions and can be performed without applied bias voltage, we maintain both site-specific selectivity and single-electron control. We extract the short range forces involved with this mechanism by subtracting the long range forces acquired on a dimer vacancy site. As a result of relaxation of the silicon lattice to accommodate negatively charged dangling bonds, we observe charge configurations of dangling bond structures that remain stable for many seconds at 4.5 K. Subsequently, we use charge manipulation to directly prepare the ground state and metastable charge configurations of dangling bond structures composed of up to six atoms.

DOI: 10.1103/PhysRevLett.121.166801

Atomic manipulation [1,2] has emerged as a powerful strategy to fabricate novel atomic physical-systems [3–5] and devices [6–9]. An important addition to this experimental toolkit would be the ability to design and control functional atomic charge configurations with single electron precision. To this end, several studies have demonstrated the ability to create, move, and controllably switch single charged species on a surface with scanning probe techniques [10–20]. One commonality of prior charge manipulation studies is that they have relied upon the application of bias voltage to induce charge transitions. In most cases, this results in a non-negligible tunneling current, whereas in principle, charge manipulation could be performed by transferring single electrons. Two recent works highlight progress in this area: Steurer *et al.* [16] have demonstrated the lateral manipulation of charge between pentacene molecules adsorbed to a NaCl thin film and Fatayer *et al.* [20] have performed charge manipulation with zA tunneling currents. One drawback of these approaches, however, is that in order to limit the tunneling current, a large tip-sample separation was required (up to several nm), thereby sacrificing spatial resolution.

Building on these efforts, we present the manipulation of charge within nanostructures engineered from silicon dangling bonds (DBs) on a hydrogen-terminated Si(100)-(2 × 1) surface. One advantage to working with DBs is that because they are midgap states, they are electronically isolated from the bulk substrate [21]. DBs can therefore localize charge without the requirement of a thin insulating film between structure and substrate, which has been essential in many previous studies [10–16,20,22,23]. Recent advances in the patterning of DBs have made it possible to create large error-free structures [24–26]. Noncontact atomic force microscopy measurements [27] have confirmed that the energy of the neutral to negative (0/−) charge transition of an isolated DB on a highly *n*-doped sample is close to the bulk Fermi level (within a few hundred meV). This enables the charge state of DBs to be selectively modified by shifting the (0/−) charge transition level above or below the bulk Fermi level with bias voltage or other nearby charged DBs [9,21,27,28]. In contrast, here we demonstrate charge state control of DBs based on a mechanical mechanism; the probe is used to manipulate the equilibrium position of the DB's host atom, making it energetically favorable to host a negative charge. Because this ability is based on short range interactions between the probe and target atom, and can be performed with zero applied bias voltage (0 V), close proximity to the sample is maintained, ensuring both site-specific selectivity and single-electron control.

Figure 1(a) displays two DBs patterned with two intervening hydrogen atoms using voltage pulses applied to the probe [29]. Pairs of DBs are known to host only a single negative charge because the Coulombic repulsion between

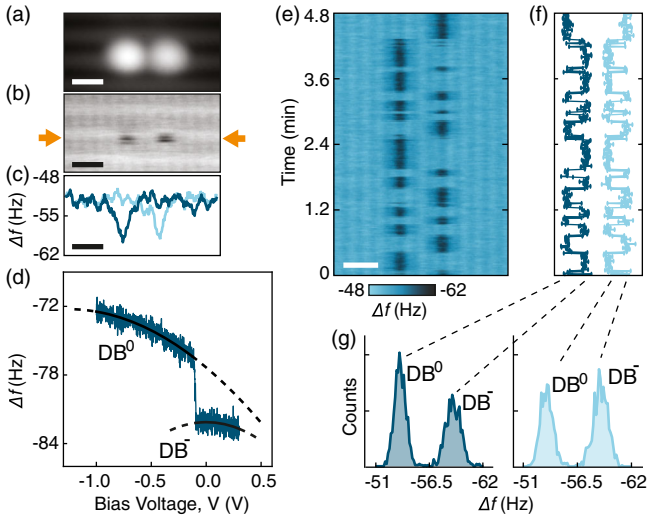

FIG. 1. Charge configurations of two closely-spaced DBs. (a) Constant current filled state STM image, −1.8 V, 50 pA. (b) Constant height Δf image, 0 V, −300 pm. (c) Two constant height Δf line scans (0 V, −300 pm) at the position indicated by the orange arrows in (b). (d) $\Delta f(V)$ spectroscopy taken above an isolated DB (−370 pm). The two individual segments have been fitted by two parabolas (solid lines: fit, dashed lines: extrapolation) corresponding to the neutral and negatively charged states (DB^0 and DB^-, respectively). (e) Combined map of 400 constant height Δf line scans (0 V, −300 pm) taken sequentially over a 4.8 minute period. (f) Time-dependent bistable signal for the two individual DBs extracted from (e). (g) Histograms of the signals in (e). Labels indicate the charge state assignment of each peak. Scale bar is 1 nm (a)–(c),(e).

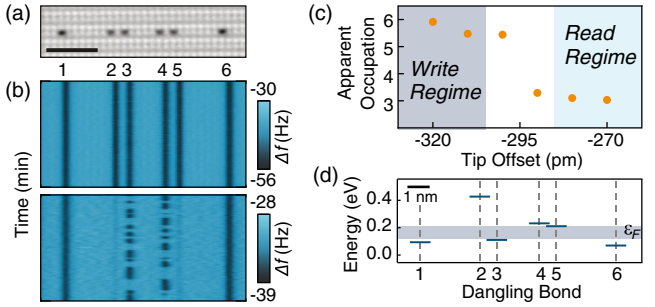

FIG. 2. Evolution of charge configurations of a symmetric six DB structure at different tip heights. (a) Constant height Δf image (0 V, −300 pm). (b) Maps of 800 constant height Δf line scans acquired over 18 minutes at −320 pm (top panel) and −270 pm (bottom panel). The scale bar in (a) is 3 nm and applies to (b). Color bars correspond to Δf. Histograms of the Δf extracted over each DB in (b) are available in Supplemental Material, Fig. S(3) [29]. (c) The average occupation of the structure inferred from digitizing the charge configuration at different Δz. Two interaction regimes: *read* and *write* are indicated. (d) Energetic shift of the $(0/-)$ levels of each DB in the structure (1, 3, and 6 are negatively charged) with respect to the $(0/-)$ level of an isolated DB (0 eV). The levels are shifted Coulombically by the negative charges confined to the structure and are calculated in the absence of the probe using an electrostatic approximation of point charges and a surface dielectric constant of 6.35. Because the exact energy of the $(0/-)$ level is unknown, we indicate a range of energies (blue shaded area) over which the bulk Fermi level would give rise to the charge configurations observed in the lower panel of (b).

two closely-spaced negative charges would otherwise be too large [21]. Here, constant height frequency shift (Δf) images of the pair appear streaky because the negative charge switches sites multiple times over the time it took to acquire an image [Fig. 1(b)]. This is seen clearly in individual Δf line scans across the structure [Fig. 1(c)] that reveal the localization of charge to one DB, with subsequent line scans demonstrating that this charge occasionally switches to the other DB. To definitively assign the contrast observed over each DB in Δf images to a charge state, we performed bias-dependent Δf spectroscopy [$\Delta f(V)$] on an isolated DB [Fig. 1(d)], which is negatively charged at 0 V on highly *n*-doped samples [27,29]. Figure 1(d) reveals a sharp transition between two parabolas [12], associated with switching between the neutral (left of the step) and negatively charged states of the DB. Comparing the Δf of the negatively charged state measured at 0 V to the extrapolation of the neutral state's parabola at 0 V confirms that the dark contrast (larger $|\Delta f|$) in Figs. 1(b),1(c) correspond to the negatively charged DB.

By stacking sequential Δf line scans [Fig. 1(f)], we monitored the charge switching between the two sites in real time. Previous theoretical estimates for the tunneling rate between two closely-spaced DBs have ranged from THz to GHz, depending on the spacing [41,42]. Surprisingly, the bistable signal for each DB extracted from Fig. 1(f) demonstrates that the system's charge configuration often remains stable for seconds [Fig. 1(g)]. Recent studies have revealed that charged species are often stabilized by a lattice relaxation of the supporting substrate [10,20,43]. Density functional theory has similarly shown that negatively charged silicon DBs experience approximately 200 meV stabilization due to a relaxation of the lattice, which results in the nuclear position of the host atom being raised by approximately 30 pm relative to the neutral state [44–46]. In this case, the lattice relaxation prevents the electron from elastically tunneling between the paired DBs. To assign the position of the charge in each Δf line scan, each trace was fitted with two Gaussian profiles. Histograms of the determined Δf center values demonstrate two Gaussian profiles, representing the negative and neutral charge states of each DB [Fig. 1(h) and Supplemental Material, Fig. S(1)] [29]. Because they are well separated, the charge state of each DB can be assigned reliably by a single line scan [Supplemental Material, Fig. S(3)] [29].

Interestingly, the occupation of DB structures observed at 0 V appears to depend strongly on Δz. Figure 2 compares a series of constant height line scan maps on a structure composed of six DBs with different Δz. The average occupation of each DB at each height can be inferred

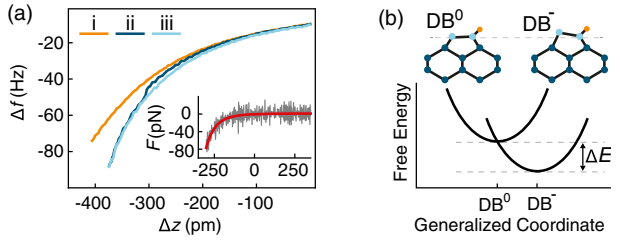

FIG. 3. Mechanically induced charge switching of a DB in a pair. (a) $\Delta f(z)$ at 0 V taken above a vacancy (i) and on a DB in a pair (ii—approach; iii—retract). Inset: the short range forces acting on the neutral DB [curve ii in (a)] up to the sharp step observed in $|\Delta f|$. See SM for more details. (b) Top panel: sketch of the equilibrium position of the host atom of a neutral DB (left) and a negatively charged DB (right). Dark blue, light blue, and orange atoms represent bulk silicon, silicon dimers, and hydrogen, respectively. Bottom panel: Free energy diagram depicting the neutral to negative charge transition for a DB due to the mechanical displacement of the host atom by the tip. ΔE corresponds to the lattice relaxation energy.

from the histograms of the Δf measured over each DB [Supplemental Material, Fig. S(3)] [29]. More simply, the average occupation of the entire structure can be inferred by counting the number of dark bars in each line scan map. At the tip's closest approach [−320 pm, top panel Fig. 2(b)] all six DBs appear negatively charged. Upon withdrawing the tip by just 50 pm [−270 pm, Fig. 2(b) bottom panel], only three DBs image as negatively charged. This change in the apparent time-averaged occupation of the structure does not vary linearly with Δz, but instead transitions sharply between −300 and −290 pm [Fig. 2(c)].

To understand this trend we performed distance-dependent Δf spectroscopy [$\Delta f(z)$] at 0 V on the individual DBs of a pair [Fig. 3(a), blue curves] and over a vacancy on the surface [Fig. 3(a), orange curve]. We began by withdrawing the tip 700 pm from the reference height [29] to effectively eliminate the forces between the tip and sample, and we subsequently walked the tip towards the sample to progressively reintroduce them. Until approximately $\Delta z = -100$ pm, all three curves are nearly identical, confirming that the long range forces (i.e., capacitive forces due to the contact potential difference, and van der Waals interaction between the large number of surface and tip atoms) are dominant [47–49]. Focusing on the approach curve obtained over the DB, at $\Delta z = -302 \pm 2$ pm there is a sudden increase in the $|\Delta f|$ (observed at $\Delta z = -301 \pm 2$ pm on the other DB). Crucially, this results in hysteresis between the approach and retract curves, with the $|\Delta f|$ measured in the latter remaining larger until approximately $\Delta z = -100$ pm. Because of the similarity between the step in the approach curve and those observed in $\Delta f(V)$ experiments [e.g., Fig. 1(d)] we attribute this phenomenon to the localization of the pair's charge to the DB beneath the tip. Two observations confirm this: if a step was observed in the $\Delta f(z)$ obtained over one DB, subsequent $\Delta f(z)$ curves taken over the same DB did not demonstrate this behavior. Instead, both the approach and retract curves trace the curve with the greater $|\Delta f|$, indicating the DB remained charged. In contrast to this behavior, if a step was observed in the $\Delta f(z)$ obtained over one DB and the subsequent $\Delta f(z)$ was performed on the other, the hysteresis was consistently observed, indicating we caused the charge to switch sites.

Similar hysteresis in $\Delta f(z)$ curves has previously been observed on the hydrogen-free Si(100) surface [50]. In their case, the presence of sudden hysteretic steps corresponded directly to a toggling of the buckling direction of a single Si(100) dimer. The authors concluded that at small absolute tip heights, short range forces between the probe and sample resulted in a mechanically-induced deformation of the lattice. The same mechanism is at play in our experiments. One distinction of our work is that the mechanical deformation also corresponds to a change in the charge state of the surface atom. This can be understood by considering the equilibrium positions of the host silicon atom for a negative and a neutral DB, which as noted earlier, differ due to the relaxation of the lattice [sketch in top panel, Fig. 3(b)] [44–46]. Because the forces are all attractive at the height corresponding to the step in the approach curve, the surface atom is displaced towards the tip, causing the atom to rehybridize and adopt greater sp^3 character. Consequently, the total free energy of the negatively charged state is lowered with respect to the neutral state, leading to the charging of the DB beneath the tip [bottom panel, Fig. 3(b)].

Because a charge manipulation mechanism based upon the mechanical manipulation of individual atoms has not been reported before, the unsuitability of electrostatic mechanisms in accounting for the results of this study must be explained. First, we note that even though the experiments were performed at 0 V, there still exists a field due to the contact potential difference. Because the work function of the Si sample is smaller than that of the W tip, this field causes states near the surface to be raised in energy relative to the bulk (i.e., upward tip-induced band bending). This effect becomes stronger with decreasing tip-sample separation; as such, the DB $(0/-)$ charge transition level remains above the bulk Fermi level, and consequently, tip-induced band bending cannot be used to explain the preferential charging of DBs beneath the tip. Screening of the local charges by the metallic tip was also considered and found to be incapable of accounting for the experimental observations [29]. Further evidence for a mechanical mechanism is found by isolating the forces acting between the tip and the DB from the total tip-sample interaction by using $\Delta f(z)$ curves obtained over dimer vacancies on the surface [Supplemental Material, Figs. S(4) and S(5)] [29] to separate the long and short range force contributions [47–49]. We found that the short range forces required to lift the equilibrium position of the neutral host atom are fit best by a function of the form $-C/z^7$, where z is

the absolute tip height and C is a constant [Supplemental Material, Fig. S(5)] [29]. This strongly suggests that van der Waals forces are responsible for displacing the host atom [51]. The functional form of the forces measured between the tip and the neutral and negatively charged DB [Supplemental Material, Fig. S(5)] also allow a charge manipulation mechanism based on an electrostatic shift of the DB $(0/-)$ charge transition level by a charged atom on the tip's apex to be ruled out with confidence [29]. A force of -75 ± 13 pN (-77 ± 12 pN) was found for the right (left) DB [inset Fig. 3(a)]. Sweetman *et al.* reported that a force in the range of 100–600 pN was required to toggle the Si dimer [50,52], and that this force corresponded to the formation of a covalent bond between the tip's apex atom and the surface atom. The comparably small force reported here is consistent with the interpretation that van der Waals forces are responsible for lifting the silicon atom in our experiments.

The experiments in Fig. 2 can now be clearly explained. At small absolute tip heights, the short range forces are strong enough that as the probe scans over the structure the charging of each DB becomes favorable whenever it is beneath the tip [top panel, Fig. 2(b)]. This necessitates that electrons vacate prior negatively charged DBs such that the overall occupation of the structure remains constant. Upon withdrawing the tip a short distance, however, this effect is greatly diminished. As a result, specific charge configurations are observed to remain stable for many sequential measurements [>15 s on average, bottom panel, Fig. 2(b)]. Another crucial observation is that only two charge configurations appear consistently: the two outer DBs remain continuously charged and a single negative charge is observed to switch between the two central DBs, similar to the behavior observed on an isolated pair. By observing that the total amount of time the central charge spends in the left DB (50%) is roughly equal to the right (46%), and noting the structure's symmetry, it is clear that these two charge configurations correspond to the degenerate ground state. Higher energy charge configurations were not observed for this structure, likely because the Coulombic interaction between closely spaced negative charges makes them energetically unfavorable, e.g., if DBs 1, 2, and 6 in Fig. 2(d) were negatively charged. We therefore identify two interaction regimes [Fig. 2(c)]: one where charge can be controllably manipulated by the tip (the *write regime*) and another where stable or metastable charge configurations can be observed (the *read regime*).

To further validate our assignment of the write and read regimes, we performed the experiments depicted in schemes Figs 4(a)–4(c) on the symmetric structure [Fig. 4(d)] and an asymmetric structure composed of five DBs [Fig. 4(h)]. First, we restricted the measurements to the read regime [schemes Figs. 4(a),4(e),4(i)], which allows us to characterize the intrinsic charge configurations of the structures and assess their relative energies based on how often they occur [histograms in Supplemental Material, Fig. S(6)] [29].

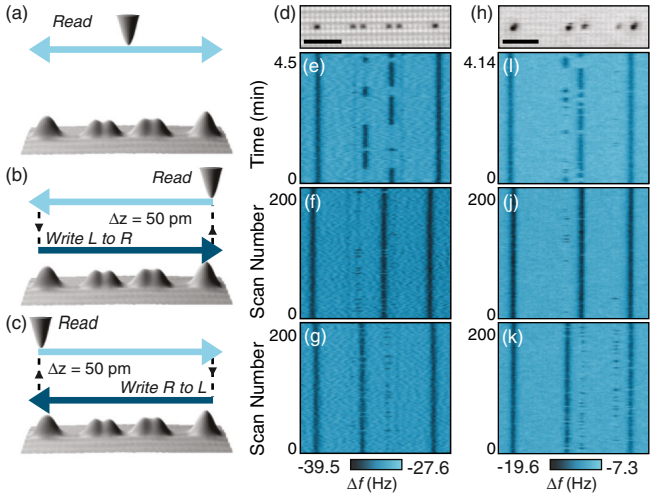

FIG. 4. Controlled preparation of charge configurations in symmetric and asymmetric DB structures. Visualization of the scan modes: (a) all measurements are restricted to the *read regime*; (b) The tip is scanned from left to right (*L to R*) in the *write regime*, retracted 50 pm to the read regime, and scanned back across; (c) the same process as (b) with directions reversed (*write R to L*). (d) Constant height Δf image of the symmetric six-DB structure (0 V, −300 pm). (e)–(g) Maps of 200 line scans across structure in (d) corresponding to scheme (a) shown in (e), scheme (b) shown in (f), and scheme (c) shown in (g) (write regime: −320 pm, read regime: −270 pm). (h) Constant height Δf image of the asymmetric five-DB structure, −350 pm, 0 V. (i)–(k) Maps of 200 line scans across structure (i) corresponding to scheme (a) (i), scheme (b) (j), and scheme (c) (k) (write regime: −370 pm, read regime: −320 pm). The scale bars in (d) and (h) are 3 nm. Data displayed in (e)–(k) correspond to the read regime of each sequence.

Subsequent experiments contained two associated phases: in the write phase, the tip was scanned across the structure at close proximity; in the read phase, the tip was retracted 50 pm with respect to the write phase and scanned back across [schemes Figs. 4(b),4(c)] to observe the prepared charge configuration. Indeed, Figs. 4(f),4(g) and 4(j),(k) confirm that charge in the interior of both structures can be manipulated. On the symmetric structure, we could consistently initiate charge to the right [Fig. 4(f) 85%] or left [Fig. 4(g) 79%] central DB, corresponding to preparation of the degenerate ground state configurations observed in Fig. 4(e). On the asymmetric structure, measurements restricted to the read regime [Fig. 4(i)] demonstrate that this system has three negative charges. On this structure, only the charge confined to the inner pair fluctuates, but because the structure is asymmetric, these two charge configurations are nondegenerate. Although we expected the interior charge to favor the left DB of the pair, because that configuration would minimize the electrostatic interaction between the three negative charges, we observe the opposite [Fig. 4(i) 18% vs 73%, respectively]. This indicates that other charged species (e.g., DBs or ionized donors) likely act as an

additional electrostatic bias on this structure. We note, however, that hidden biases can be counteracted by patterning additional DBs in the area surrounding DB structures [Supplemental Material, Fig. S(7)] [29]. Using the techniques previously described the central charge could be manipulated to selectively occupy the right [Fig. 4(j) 92%] or left [Fig. 4(k) 67%] DB of the pair, demonstrating that in addition to the ground state configurations the occurrence of metastable charge configurations can also be enhanced [Fig. 4(i)].

These results demonstrate that single electrons can be manipulated within structures derived from DBs by using the probe to mechanically manipulate the equilibrium position of the host atoms. Underlying this charge control mechanism is relaxation of the silicon lattice, which acts to stabilize negatively charged DBs. The techniques presented here expand the scanning probe toolkit with the ability to position charge within atomic structures to prepare desired charge configurations.

We would like to thank Mark Salomons and Martin Cloutier for their technical expertise. We also thank Leo Gross and Gerhard Meyer for stimulating discussions. We thank NRC, NSERC, and AITF for their financial support.

M. R., W. V., and T. D. contributed equally to this work.

*rashidi@ualberta.net
†Current address: Centre for Quantum Computation and Communication Technologies, School of Electrical Engineering and Telecommunications, UNSW, Sydney, New South Wales 2052, Australia.
wyattvine@gmail.com
‡thdienel@gmail.com

[1] D. K. Schweizer and E. K. Eigler, Nature (London) **344**, 524 (1990).
[2] Y. Sugimoto, P. Pou, O. Custance, P. Jelinek, M. Abe, R. Perez, and S. Morita, Science **322**, 413 (2008).
[3] M. R. Slot, T. S. Gardenier, P. H. Jacobse, G. C. P. van Miert, S. N. Kempkes, S. J. M. Zevenhuizen, C. M. Smith, D. Vanmaekelbergh, and I. Swart, Nat. Phys. **13**, 672 (2017).
[4] R. Drost, T. Ojanen, A. Harju, and P. Liljeroth, Nat. Phys. **13**, 668 (2017).
[5] S. Fölsch, J. Martínez-Blanco, J. Yang, K. Kanisawa, and S. C. Erwin, Nat. Nanotechnol. **9**, 505 (2014).
[6] A. A. Khajetoorians, J. Wiebe, B. Chilian, and R. Wiesendanger, Science **332**, 1062 (2011).
[7] M. Fuechsle, J. A. Miwa, S. Mahapatra, H. Ryu, S. Lee, O. Warschkow, L. C. L. Hollenberg, G. Klimeck, and M. Y. Simmons, Nat. Nanotechnol. **7**, 242 (2012).
[8] F. E. Kalff, M. P. Rebergen, E. Fahrenfort, J. Girovsky, R. Toskovic, J. L. Lado, J. Fernández-Rossier, and A. F. Otte, Nat. Nanotechnol. **11**, 926 (2016).
[9] T. Huff, H. Labidi, M. Rashidi, R. Achal, L. Livadaru, T. Dienel, J. Pitters, and R. A. Wolkow, arXiv:1706.07427.
[10] J. Repp, G. Meyer, F. E. Olsson, and M. Persson, Science **305**, 493 (2004).
[11] G. V. Nazin, X. H. Qiu, and W. Ho, Phys. Rev. Lett. **95**, 166103 (2005).
[12] L. Gross, F. Mohn, P. Liljeroth, J. Repp, F. J. Giessibl, and G. Meyer, Science **324**, 1428 (2009).
[13] M. Sterrer, T. Risse, U. M. Pozzoni, L. Giordano, M. Heyde, H. P. Rust, G. Pacchioni, and H. J. Freund, Phys. Rev. Lett. **98**, 096107 (2007).
[14] T. Leoni, O. Guillermet, H. Walch, V. Langlais, A. Scheuermann, J. Bonvoisin, and S. Gauthier, Phys. Rev. Lett. **106**, 216103 (2011).
[15] W. Steurer, J. Repp, L. Gross, I. Scivetti, M. Persson, and G. Meyer, Phys. Rev. Lett. **114**, 036801 (2015).
[16] W. Steurer, S. Fatayer, L. Gross, and G. Meyer, Nat. Commun. **6**, 8353 (2015).
[17] S. D. Bennett, L. Cockins, Y. Miyahara, P. Grutter, and A. A. Clerk, Phys. Rev. Lett. **104**, 017203 (2010).
[18] K. Teichmann, M. Wenderoth, S. Loth, J. K. Garleff, A. P. Wijnheijmer, P. M. Koenraad, and R. G. Ulbrich, Nano Lett. **11**, 3538 (2011).
[19] M. Setvin, J. Hulva, G. S. Parkinson, M. Schmid, and U. Diebold, Proc. Natl. Acad. Sci. U.S.A. **114**, E2556 (2017).
[20] S. Fatayer, B. Schuler, W. Steurer, I. Scivetti, J. Repp, L. Gross, M. Persson, and G. Meyer, Nat. Nanotechnol. **13**, 376 (2018).
[21] M. B. Haider, J. L. Pitters, G. A. DiLabio, L. Livadaru, J. Y. Mutus, and R. A. Wolkow, Phys. Rev. Lett. **102**, 046805 (2009).
[22] L. Liu, T. Dienel, R. Widmer, and O. Gröning, ACS Nano **9**, 10125 (2015).
[23] F. Schulz, M. Ijäs, R. Drost, S. K. Hämäläinen, A. Harju, A. P. Seitsonen, and P. Liljeroth, Nat. Phys. **11**, 229 (2015).
[24] N. Pavliček, Z. Majzik, G. Meyer, and L. Gross, Appl. Phys. Lett. **111**, 053104 (2017).
[25] T. R. Huff, H. Labidi, M. Rashidi, M. Koleini, R. Achal, M. H. Salomons, and R. A. Wolkow, ACS Nano **11**, 8636 (2017).
[26] R. Achal, M. Rashidi, J. F. Croshaw, D. Churchill, M. Taucer, T. Huff, M. Cloutier, J. Pitters, and R. A. Wolkow, Nat. Commun. **9**, 2778 (2018).
[27] M. Rashidi, E. Lloyd, T. R. Huff, R. Achal, M. Taucer, J. J. Croshaw, and R. A. Wolkow, ACS Nano **11**, 11732 (2017).
[28] M. Taucer, L. Livadaru, P. G. Piva, R. Achal, H. Labidi, J. L. Pitters, and R. A. Wolkow, Phys. Rev. Lett. **112**, 256801 (2014).
[29] See Supplemental Material at http://link.aps.org/supplemental/10.1103/PhysRevLett.121.166801, which includes Refs. [25,30–40], for methods, definition and discussion of error rate, data processing for repeated line scan experiments and assignment of digital charge configurations, height-dependent contrast in Δf images, frequency to force conversion, discussion of charge manipulation mechanisms based on electrostatics, as well as additional experimental data.
[30] F. J. Giessibl, Appl. Phys. Lett. **76**, 1470 (2000).
[31] J. E. Sader and S. P. Jarvis, Appl. Phys. Lett. **84**, 1801 (2004).
[32] J. Welker, E. Illek, and F. J. Giessibl, Beilstein J. Nanotechnol. **3**, 238 (2012).
[33] M. Rezeq, J. Pitters, and R. Wolkow, J. Chem. Phys. **124**, 204716 (2006).
[34] H. Labidi, M. Koleini, T. Huff, M. Salomons, M. Cloutier, J. Pitters, and R. A. Wolkow, Nat. Commun. **8**, 14222 (2017).

[35] S. Jarvis, A. Sweetman, J. Bamidele, L. Kantorovich, and P. Moriarty, Phys. Rev. B **85**, 235305 (2012).
[36] J. L. Pitters, P. G. Piva, and R. A. Wolkow, J. Vac. Sci. Technol., B **30**, 021806 (2012).
[37] M. Rashidi, J. A. J. Burgess, M. Taucer, R. Achal, J. L. Pitters, S. Loth, and R. A. Wolkow, Nat. Commun. **7**, 13258 (2016).
[38] J. W. Lyding, T. C. Shen, J. S. Hubacek, J. R. Tucker, and G. C. Abeln, Appl. Phys. Lett. **64**, 2010 (1994).
[39] S. R. Schofield, N. J. Curson, J. L. O'Brien, M. Y. Simmons, R. G. Clark, N. A. Marks, H. F. Wilson, G. W. Brown, and M. E. Hawley, Phys. Rev. B **69**, 085312 (2004).
[40] N. J. Curson, S. R. Schofield, M. Y. Simmons, L. Oberbeck, J. L. O'Brien, and R. G. Clark, Phys. Rev. B **69**, 195303 (2004).
[41] L. Livadaru, P. Xue, Z. Shaterzadeh-Yazdi, G. A. DiLabio, J. Mutus, J. L. Pitters, B. C. Sanders, and R. A. Wolkow, New J. Phys. **12**, 083018 (2010).
[42] Z. Shaterzadeh-Yazdi, B. C. Sanders, and G. A. DiLabio, J. Chem. Phys. **148**, 154701 (2018).
[43] F. E. Olsson, S. Paavilainen, M. Persson, J. Repp, and G. Meyer, Phys. Rev. Lett. **98**, 176803 (2007).
[44] J. E. Northrup, Phys. Rev. B **40**, 5875 (1989).
[45] S. R. Schofield, P. Studer, C. F. Hirjibehedin, N. J. Curson, G. Aeppli, and D. R. Bowler, Nat. Commun. **4**, 1649 (2013).
[46] H. Kawai, O. Neucheva, T. Leh, C. Joachim, and M. Saeys, Surf. Sci. **645**, 88 (2016).
[47] M. A. Lantz, H. J. Hug, R. Hoffmann, P. J. A. van Schendel, P. Kappenberger, S. Martin, A. Baratoff, and H.-J. Güntherodt, Science **291**, 2580 (2001).
[48] M. Ternes, C. González, C. P. Lutz, P. Hapala, F. J. Giessibl, P. Jelínek, and A. J. Heinrich, Phys. Rev. Lett. **106**, 016802 (2011).
[49] A. Sweetman and A. Stannard, Beilstein J. Nanotechnol. **5**, 386 (2014).
[50] A. Sweetman, S. Jarvis, R. Danza, J. Bamidele, S. Gangopadhyay, G. A. Shaw, L. Kantorovich, and P. Moriarty, Phys. Rev. Lett. **106**, 136101 (2011).
[51] F. Bocquet, L. Nony, and C. Loppacher, Phys. Rev. B **83**, 035411 (2011).
[52] S. Jarvis, A. Sweetman, J. Bamidele, L. Kantorovich, and P. Moriarty, Phys. Rev. B **85**, 235305 (2012).

Supplemental Material:
Initiating and monitoring the evolution of single electrons within atom-defined structures

Mohammad Rashidi[1,2,3*], Wyatt Vine[1*], Thomas Dienel[1,2*], Lucian Livadaru[3], Jacob Retallick[4], Taleana Huff[1,3], Konrad Walus[4], Robert A. Wolkow[1,2,3]

[1]Department of Physics, University of Alberta, Edmonton, AB, Canada, T6G 2R3

[2]Nanotechnology Initiative, Edmonton, AB, Canada, T6G 2M9

[3]Quantum Silicon, Edmonton, AB, Canada, T6G 2M9

[4]Department of Electrical and Computer Engineering, University of British Columbia, Vancouver, BC, Canada, V6T 1Z4

*Authors contributed equally

Correspondence to: rashidi@ualberta.net, wyattvine@gmail.com, thdienel@gmail.com

Table of Contents:

Methods: All experiments were performed on an Omicron LT STM/AFM operating at 4.5 K and ultrahigh vacuum ($< 1 \times 10^{-10}$ Torr). Tips were created from polycrystalline tungsten wire that was chemically etched, sharpened with a focused ion beam, and attached to a qPlus sensor [30]. The tips had resonance frequencies of 28 kHz, Q-factors between 12k and 14k, and were driven with an amplitude of 50 pm. Frequency shift measurements were converted to force using the Sader-Jarvis method [31,32]. A stiffness of 1800 N/m for the frequency shift to force conversion was assumed. An additional electrode on the sensor was used to supply tunneling current. Tips were further sharpened by nitrogen etching while performing field ion microscopy [33]. *In-situ* tip processing was performed by controlled contacts of the tip to the sample surface which likely results in a decoration of the tip apex with silicon atoms [25,34,35]. Samples were cleaved from highly arsenic doped (1.5×10^{19} atom/cm^3) (100)-oriented Si crystals. After degassing at 600^{o}C for 12 hours, samples were flash annealed to temperatures as high as 1250^{o}C before passivating the surface with hydrogen while maintaining a sample temperature of 330^{o}C. The high flash temperatures have been previously shown to induce a dopant depletion region extending as far as 100 nm below the sample surface [36,37]. DBs were patterned by applying short voltage pulses (+2.1 V, 10 ms) with the tip positioned directly above hydrogen [38]. All tip offsets (Δz) used within the manuscript are in reference to an STM setpoint of -1.8 V and 50 pA measured over hydrogen.

Error Rate: Throughout measurements restricted to the *read*-regime we occasionally observed negative charges occupying both dangling bonds in a pair, despite this being unlikely due to Coulombic repulsion. We define these line scans as errors. While it was typically several percent we have achieved error rates of <1% (Supporting Information, Fig. S2). We have identified several contributing factors. (*i*) The *read* and *write* regimes are sensitive to the tip height (Fig. 2 and SI Fig. S3). Accordingly, we find that small changes in tip height (*e.g.* noise of the tuning fork's amplitude) can occasionally result in unintentional manipulation of the charge state of dangling bonds beneath the tip while in the *read*-regime. This can result in an increase to the apparent occupation of the structure (*e.g.* Fig. 2). It can also reduce the success-rate of charge manipulation in the *write*-regime. (*ii*) Sharp tips were found to more clearly resolve the two charge states of each dangling bond, *i.e.*, better signal to noise ratio. This reduces the number of incorrect charge state assignments, which are performed in a digital fashion. Similarly, with H-terminated tips, which can be effectively identified via force distance spectroscopy [25], it was more difficult to discriminate the two charge states of each dangling bond.

Data processing for repeated line scan experiments and assignment of digital charge configurations: Minimal data processing was performed, and raw data was used whenever possible. All experiments with repeated line scans were performed in constant height mode. For experiments performed entirely in the *read* regime, forward and backward line scans, which are saved in separate files by the control software, were aligned manually by removing an equal number of pixels at the start of both scans and zipped together (step 1, Fig. S1b). Measurements often exceeded 30 minutes, over which time the tip would inevitably drift towards or away from the surface due to piezo creep and thermal drift. To account for this, a linear drift was subtracted from all measurements with repeated line scans by fitting the average Δf for each line scan over the course of an experiment (step 2, Fig. S1c). In experiments where Δf drifted by more than 2 Hz the entire run was rejected.

The Δf value measured over each dangling bond was extracted by independently fitting each dangling bond associated peak in the line scans (defined by a 30-pixel window centered on their position) with a Gaussian function (step 3, Fig. S1d). Supporting Figure S1e,f shows the extracted Δf values for two dangling bonds. The bistable behavior of each dangling bond is clearly visible.

Binary numbers were assigned to the charge states by making a single cut in Δf (Fig. S1e,f demonstrate cuts). Dangling bonds with $|\Delta f|$ greater than the cut were assigned a negative charge state, while those with $|\Delta f|$ smaller than the cut were assigned a neutral charge state (Fig. S1e,f). Two additional steps were used to create the histograms in Fig. S3 and S4. First, the smallest $|\Delta f|$ in the set of the Δf extracted for all the dangling bonds in an experiment (corresponding to a fit of the background) was set to 0 (step 4). Thus, the normalized Δf for all the dangling bonds would be positive. Second, each Δf was normalized by setting the average Δf for the two isolated dangling bonds to 1.0 (step 5). Because the isolated dangling bonds were always negatively charged, a normalized Δf of 1.0 corresponds to the average Δf for a negatively charged dangling bond. Similar to the process above a single common cut in Δf was used to assign charge states to the normalized data (step 6).

Height-dependent contrast in Δf images: To provide additional insight to the qualitative behaviour of the Δf signal above each species we measured site-specific force curves. The results are presented as Figure 3a and in Supporting Figure S5 which shows $\Delta f(z)$ signals obtained while approaching the tip to the corresponding sites. For large tip-surface separations (height range >0 pm) all three species exhibit an identical frequency shift, *i.e.* the $\Delta f(z)$ curves coincide and there is no contrast. As the tip approaches (approx. -200 to 0 pm), attractive van der Waals forces are observed first on the hydrogen atoms. As a result, vacancies and neutral DBs have smaller $|\Delta f|$ compared to the surrounding H atoms and appear as bright protrusions in Δf images taken in this height range. Negatively charged DBs appear dark (large $|\Delta f|$) due to electrostatic contributions.

For tip offsets closer to the surface than -200pm, the tip enters the repulsive regime over hydrogen atoms. Consequently, the $|\Delta f|$ obtained over the neutral dangling bond becomes greater than that of the hydrogen resulting in a darker appearance of the DBs. The final feature of interest is a sharp step (approx. -300 pm) in the approach curve on the neutral DB, which we attribute to the charging of the dangling bond beneath the tip and the dark appearance (large $|\Delta f|$). As the tip is being retracted the charge remains at the site under the tip and the corresponding DB appears darker than hydrogen or neutral DBs in Δf images. All images and line profiles for the *write* and *read* scans are well within the same height regime and no contrast inversion exists.

Frequency to force conversion: To reliably separate the short range forces measured over dangling bonds and hydrogen we took reference measurements over dimer vacancies (Fig. S4). [39, 40] We performed our measurements of $\Delta f(z)$ at the various sites in a series while keeping the instrument in constant height mode. Repeatedly taking $\Delta f(z)$ spectra over hydrogen atoms throughout the experiment allowed us to determine the residual thermal drift and piezo artefacts. Afterwards we shifted the spectra relative to one another and calculated the minimum residual sum squared error of the shifted spectra

$$\Sigma\ (\Delta f(z)_{shifted} - \Delta f(z)_{reference})^2 .$$

By comparing the determined optimum offset for each hydrogen spectrum we revealed linear drift within each set of measurements, which subsequently allows us to correct the tip offsets.

We used the Sader-Jarvis method [31] and corrections proposed by welker and Giessibl [32] to convert the $\Delta f(z)$ spectra to force curves (Fig. S5). We assumed a cantilever stiffness of 1800 N/m but note that others have reported large uncertainties in this value. The uncertainty in our reported short range forces correspond to the standard deviation between the data and their optimal fit and so a linear correction to the forces and their corresponding uncertainties would result if a different stiffness was assumed.

Discussion of charge manipulation mechanisms based on electrostatics: In order to understand our experimentally observed charge manipulation ability we first considered mechanisms based on electrostatic effects. In the following we justify why these are not suitable for describing our experimental results:

1) With the exception of the KPFM spectra displayed as Figure 1d, all of the experiments presented were performed at zero applied bias voltage. Nonetheless, an electric field exists under the AFM tip as a result of the contact potential difference, arising as a result of the difference in the work

functions of the tip (~4.8 eV) and sample (4.1 eV). At zero applied bias voltage the overall contact potential difference is therefore on the order of -700 meV (referenced to the sample), which results in the bands near the surface being shifted higher in energy relative to the bulk crystal (*aka* tip induced band bending). We note that the assumed contact potential difference is consistent with the KPFM spectroscopy results. This effect becomes more pronounced as the tip approaches because a smaller proportion of the effective voltage is dropped across the vacuum gap. In this way, bringing the tip closer to a neutral DB would result in the DB's (0/-) charge transition level being raised in energy, and therefore the DB would remain neutral. In our experiments, we observe the opposite effect, *i.e.* that by bringing the tip closer to a neutral DB we are able to make it negatively charged, meaning that the DB's (0/-) charge transition level goes below the Fermi level. Therefore the charging of a neutral DB at 0 V by the tip cannot be explained by tip induced band bending alone.

2) One must also consider that, because the tip is metallic, it will partially screen the local charges. Our modeling of this effect considered the image charge that a negatively charged DB would induce within the metallic tip. Because in our case the dangling bonds are negatively charged, the image charge would be positive. The effect of this image charge would therefore be to contribute a positive field component that would counteract the contact potential difference. If the field originating from the image charge were sufficiently strong it could overcome the contact potential difference, leading to overall downward band bending at the surface. In this case the DB beneath the tip could become negatively charged.

   To understand how this mechanism would manifest in our experiments, let us consider as an example, a charge manipulation experiment performed on a structure comprised of two closely-spaced DBs. Recall that such a pair hosts a single net negative charge, and assume that the charge is currently in the left-hand DB. If the charge screening effect were responsible for the charge manipulation mechanism, we require that by placing the tip over the site of the right-hand DB and moving it towards the sample by 50 pm the effect of the image charge becomes sufficiently strong to push the right-hand DB's (0/-) charge transition level below the Fermi level (at which point the structure's charge configuration would change). When we modelled this scenario we found that while the image charge component does get stronger as the tip approaches, so too does the tip induced band bending. In many scenarios, the magnitudes of these two field components at the surface actually increased similarly, preventing the image charge effect from pushing the right-hand DB's (0/-) charge transition level below the Fermi level. Furthermore, the lateral extent of the image charge potential was too broad in order to energetically favor an individual DB over its neighbor, thus contradicting the experimentally observed site selectivity.

   In order to find a regime where the image charge effect could conceivably result in *writing* we had to tightly constrain several inputs to our model (the contact potential difference, the tip's apex radius, the tip's absolute height, the surface dielectric constant, the effective dielectric constant experienced by the image charge, etc.). In addition, the values of these parameters were not consistent between models of experiments on structures with different numbers of DBs, contrasting our experiments where we could use the same tip to perform charge manipulation on

different DB structures. For these reasons, we are confident that the image charge effect cannot be used to explain charge manipulation in our experiments.

3) Another conceivable explanation is that a positively charged atom on the tip (perhaps an impurity) could electrostatically shift the DB (0/-) charge transition level below the Fermi level, thereby causing it to be negatively charged. We are convinced it cannot be the mechanism responsible in our experiments for two reasons:

    A) The results contained within the manuscript were obtained with several distinct tips. Above we have noted that the charge manipulation experiments benefit from sharp tips because they increase contrast among the two charge states in the Δf signal (also that hydrogen-functionalization seems to decrease the contrast). Otherwise we have not performed any special tip-processing or noted any imaging qualities that would suggest the requirement of specially functionalized tips.

    B) We do not observe the characteristic interactions between a charged apex atom and a charged/neutral dangling bond are reflected within the force measurements included in the inset of Figure 3a and Figure S5. If the apex atom were charged we would expect the force corresponding to the tip approaching a neutral dangling bond to have a $1/r^5$ dependence, corresponding to a predominant ion-dipole interaction. Instead we find that the force curve is best fit by a function of the form $1/r^7$, strongly suggesting the interaction is van der Waals. Similarly we find the interaction between a negatively charged DB and the tip is best fit by a function of the form $1/r^5$, suggesting an ion-dipole interaction, whereas we would expect a $1/r^2$ force if both atoms were charged. Both of these observations are therefore consistent with the tip's apex atom being neutral.

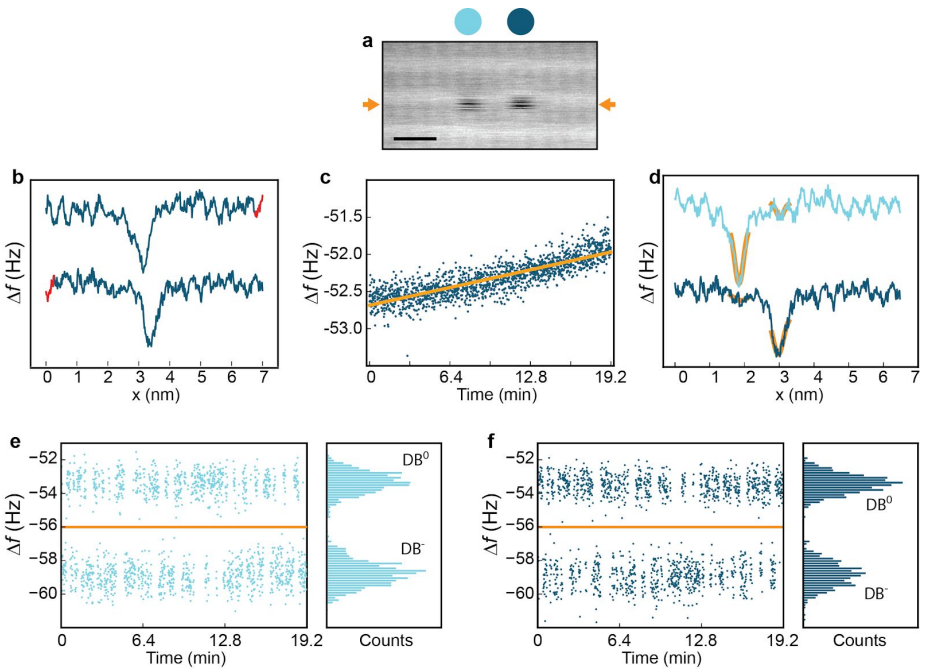

Figure S1: Illustration of data processing routine for Δ*f* maps. (**a**) Constant height Δ*f* image of a dangling bond structure taken at 0 V. The initial tip height is set on a hydrogen atom at -1.8 V and 50 pA before moving the tip 300 pm towards the surface. The scale bar is 1 nm. (**b**) Two sequential Δ*f* line scans demonstrate negative charge confined to the right-hand dangling bond (line scan width is larger than the window shown in (a), line scans are offset for clarity). The peaks are not aligned because they correspond to forward (top) and backward (bottom) line scans, which typically have a fixed offset due to piezo creep. The red tails on both line scans demonstrate the data that is chopped to align the scans. (**c**) The average Δ*f* of each line scan over the course of the entire experiment demonstrates that the tip was slowly drifting away from the sample. A linear fit of this data (orange line) is subtracted from the dataset. (**d**) Each line scan is fit with two gaussian peaks to extract the Δ*f* over each dangling bond (colour legend indicated above (a)). Note that for neutral dangling bonds this corresponds to a fit of the signal associated with hydrogen/noise. (**e-f**) The Δ*f* extracted for each dangling bond clearly displays two distinct states, which we assign to the negative and neutral charge states of each dangling bond. Each histogram has 75 equal width bins between Δ*f* = -62 and -51 Hz, and has an integrated area of 1.0.

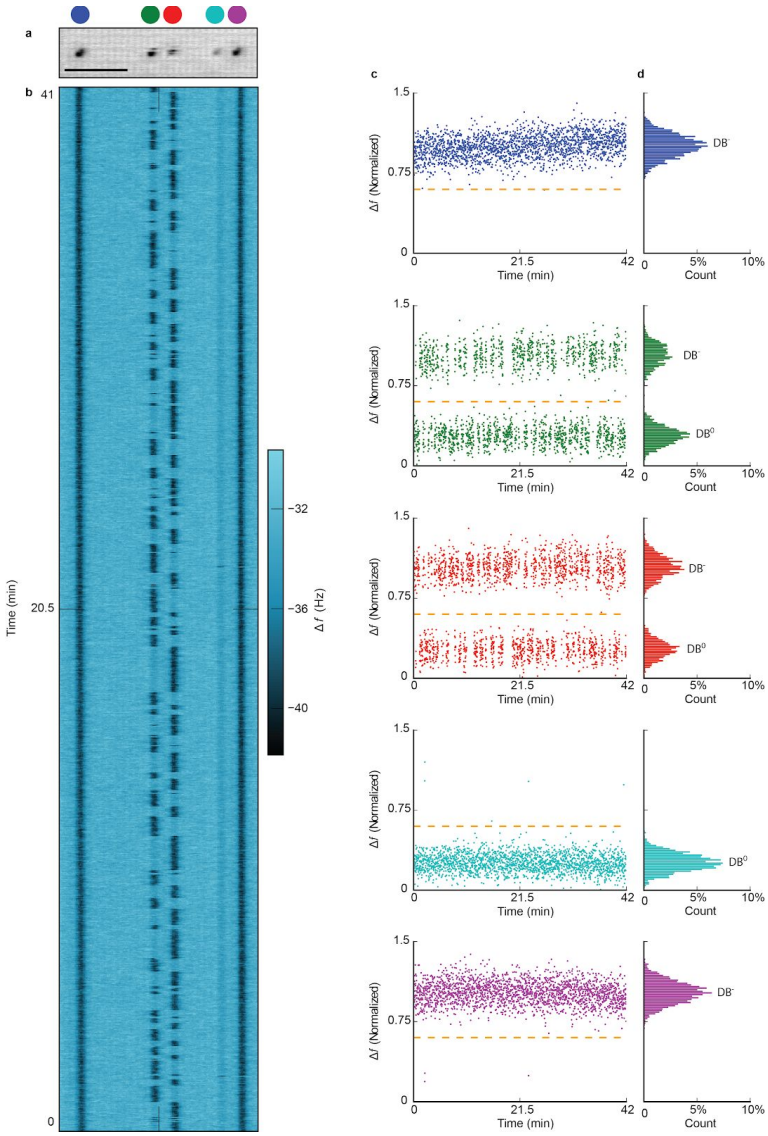

Figure S2: Digitization of line scans of an asymmetric structure composed of five dangling bonds. (**a**) Constant height Δf image of the dangling bond structure at 0 V. (**b**) A line scan map composed of 2048 Δf line scans acquired in the *read*-regime (-300 pm) over structure demonstrate. (**c**) The normalized Δf acquired over each dangling bond throughout the course of the experiment demonstrates clearly that there are two charge states of each dangling bond (although only the green and red dangling bonds appear to fluctuate between them). With the normalizing procedure described above the negative dangling bond charge state is normalized to a Δf of 1.0, and the Δf of the neutral dangling bond state is centered approximately at 0.25. The orange dotted lines demonstrate that a single common cut of Δf = 0.6 in the normalized data can be used to digitize the charge state of the structure with each line scan. (**d**) Histograms of the normalized Δf for each dangling bond reveal that the Δf corresponding to the two charge states of each dangling bond have a Gaussian distribution. Upon assigning binary numbers to this dataset it was found that in <1% of the line scans the charge configuration corresponded to having a third negative charge in the four paired dangling bonds. Each histogram has 75 equal width bins between Δf(normalized) = 0 and 1.5, and has an integrated area of 1.0.

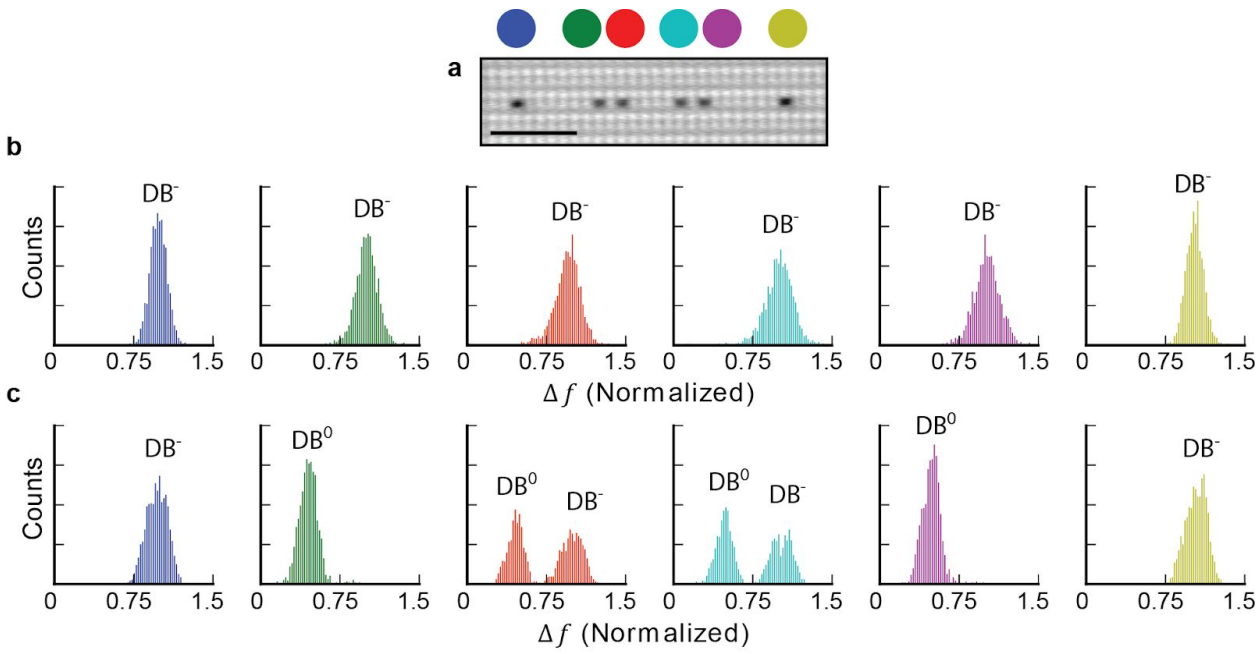

Figure S3: Histograms of the normalized Δ*f* measured over each site in a symmetric six dangling bond structure at different tip heights. (**a**) Constant height Δ*f* image of the structure. (**b**, **c**)Histograms of the normalized Δ*f* measured over each dangling bond at (b) z = -320 pm and (c) z = -270 pm. 1600 line scans at both heights were used to gather statistics. Each histogram has 75 equal width bins between Δ*f*(normalized) = 0 and 1.5, and has an integrated area of 1.0. All the dangling bonds appear negatively charged in (b). In (c), the isolated dangling bonds on either end (blue and yellow) remain negatively charged while the outer atoms of each pair (green and purple) are neutral. In (c) the inner atoms (red and cyan) fluctuate between the neutral and negative charge states; the integrated area of each peak is approximately 0.5, indicating they are equally likely to be in the neutral or negative charge state. This can be seen directly in Fig. 2d where a single electron switches between these two dangling bonds.

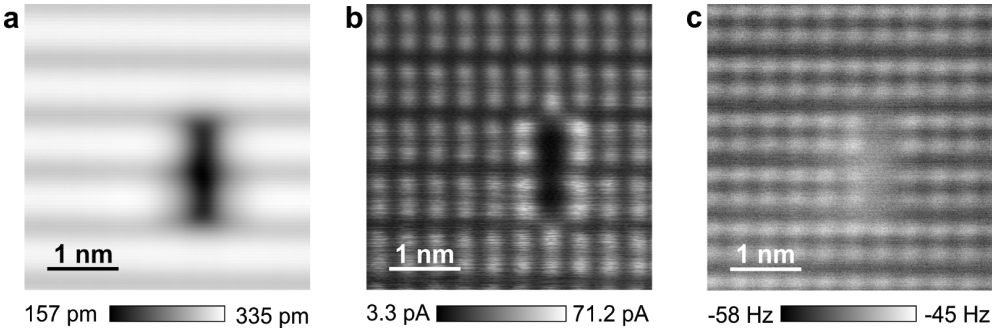

Figure S4: Dimer vacancy in neighboring dimer rows on hydrogen-terminated Si(100). (**a**) Constant current filled state STM image, -1.8V and 50 pA. (**b**) Constant height tunneling current image (300 mV, tip offset -370 pm). (**c**) Constant height Δ*f* image, 0V and tip offset -300 pm. Reference tip height for (b) and (c) is -1.8 V and 50 pA measured above hydrogen.

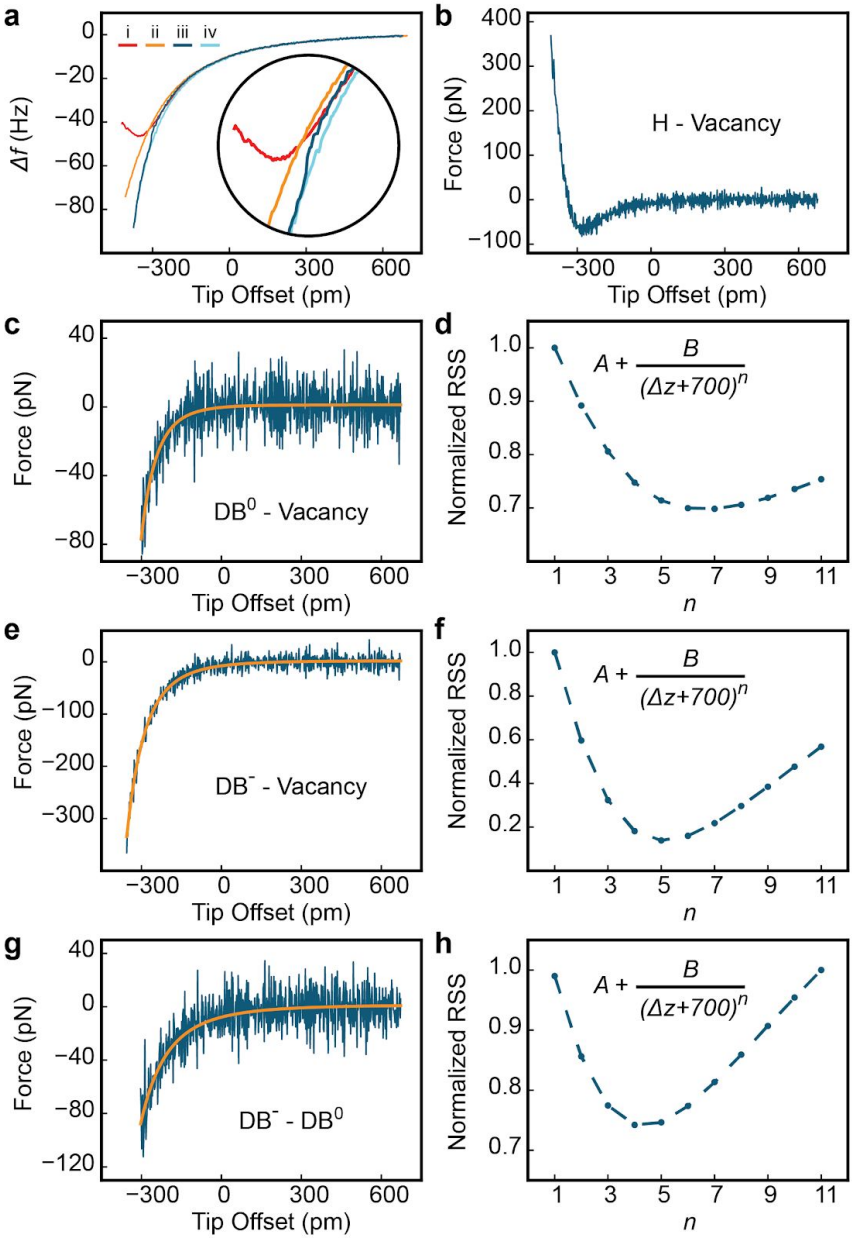

Figure S5: Extraction of short range forces from Δ*f(z)* spectra. (a) Δ*f(z)* taken over a hydrogen atom (i. red), dimer vacancy (ii. orange) and the right dangling bond of a pair (iii. dark blue, approach; iv. light blue, retract). Δ*z* = 0 corresponds to an STM setpoint of-1.8 V and 50 pA. All curves were taken at 0 V. Inset: a closeup of the spectra near Δ*z* = -300 pm. **(b)** The short range force measured over a hydrogen atom, corresponding to the difference in the force measured over the hydrogen atom and the dimer vacancy (forces found by converting Δ*f(z)* to force *via* Sader-Jarvis Method [31,32]. **(c, e, g)** The short range forces measured over a neutral and negatively charged dangling bond. The force for the neutral dangling bond corresponds to the approach curve in (a) (dark blue) up to the point of the sudden increase in |Δ*f*|. The force for the negatively charged dangling bond corresponds to the retract curve in (a) (light blue). **(d, f, h)** Comparisons of the fits of the extracted short range forces for (c, e, g), respectively. RSS corresponds to the residual sum of squares error. The absolute tip height at the set point was determined to be 700 pm. Approaching the tip 700 pm from our setpoint typically results in sudden increases to the tunneling current and small changes to the tip apex and surface, strongly suggesting the tip makes direct contact with the hydrogen-free silicon surface.

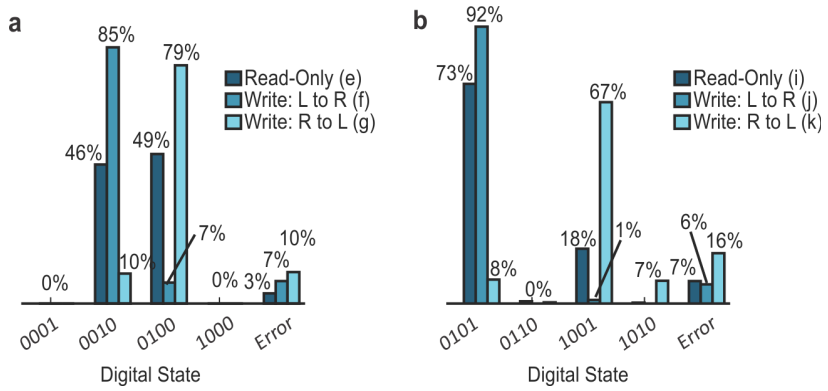

Figure S6: Histograms of the binary numbers determined from digitization of the line scans in Fig. 4. (a) and (b) depicts the histograms for Fig. 4e-g and Fig. 4i-k, respectively. 0's and 1's correspond to neutral and negatively charged DBs, respectively. Only the four interior DBs are considered.

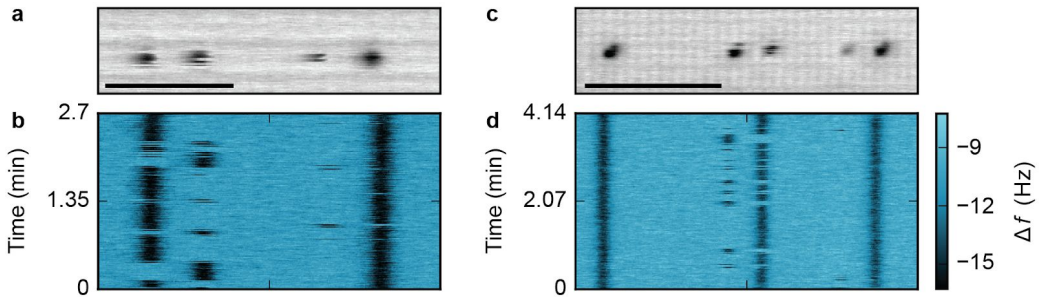

Figure S7: The influence of adding an isolated dangling bond on the polarization of dangling bond pairs. (**a**) Constant height Δf image of a symmetric structure composed of four dangling bonds. (**b**) A line scan map composed of two hundred sequential Δf line scans acquired over the structure demonstrate that it is naturally polarized. The negative charge confined to the left-hand pair favors the outer dangling bond but occasionally fluctuates to the inner dangling bond. The negative charge confined to the right-hand pair almost exclusively occupies the outer dangling bond. (**c**) An isolated dangling bond was added to the left of the *same* structure in (a) using STM lithography. (**d**) A line scan map composed of two hundred sequential Δf line scans acquired over the structure demonstrate the effect of this additional negative charge to the polarization of the structure. The right-hand pair remains polarized in the same way as (b). The polarization of the left-hand pair reverses compared to (b). This is easily rationalized by noting that the new dangling bond acts as a local Coulombic bias. This demonstrates that local charges (*e.g.* negatively charged dangling bonds or ionized donors) can influence the distribution of charge configurations these structures display. The scale bars in (a) and (c) are 3 and 4 nm, respectively. The individual line scans acquired in (d) are longer than in (b) due to the increased distance the tip has to move. The Δf colour bar applies to both (b) and (d).